Lu-Fano plot for interpretation of the photoassociation spectra

V. Kokoouline
Department of Physics and JILA, University of Colorado, Boulder, Colorado 80309-0440

C. Drag, P. Pillet, and F. Masnou-Seeuws
Laboratoire Aimé Cotton, Université Paris XI and CNRS II, Orsay 91405, France
(Received 18 December 2001; published 7 June 2002)

Recently, the method of Lu-Fano plots was extended to potentials with general R^{-n} asymptotic behavior. The aim of this paper is to discuss the efficiency of this method for the interpretation of experimental vibrational spectra of long-range diatomic molecules when two channels are coupled. A Lu-Fano analysis is implemented on experimental data for the Cs_2 $0_u^+(6S+6P_{1/2,3/2})$ photoassociation spectra below the $6S+P_{1/2}$ and $6S+P_{3/2}$ dissociation limits. The parameters are fitted on level energies and predissociation widths, giving information about the asymptotic coefficients C_3 for both channels and about a coupling parameter which determines the variation of predissociation widths as a function of detuning. This parameter can be extrapolated above the $6S+P_{3/2}$ threshold to yield the fine-structure transition cross section between the two channels. The probability for such a transition in a model where hyperfine structure effects are neglected is found to be 0.54.

DOI: 10.1103/PhysRevA.65.062710 PACS number(s): 34.20.−b, 33.80.Gj, 33.20.−t, 34.20.Mq

I. INTRODUCTION

Photoassociation spectroscopy in a sample of laser-cooled alkali-metal atoms has proven to be a very accurate tool for extracting information on the long-range interaction between atoms, yielding in particular, through the C_3 coefficient, precise radiative lifetimes for the first ^2P level of the alkali-metal atoms [1–6]. Once a rovibrational progression is unambiguously identified in the spectrum, various methods have been considered to fit molecular potentials to the measured energy levels and rotational constants. The difficulty lies in the determination of accurate potentials at short range, and can be overcome by use of purely asymptotic methods, such as the long-range analysis proposed by Le Roy and Bernstein [7]. The latter method is very efficient in case of levels close to the dissociation limit, as was demonstrated recently for the Ca photoassociation spectra [8]. Such a method assumes that no perturbation is present for the state considered, the levels corresponding to vibrational motion in a single channel. However, many observed spectra are more complex and require a multichannel analysis. The aim of the present paper is to show that generalized Lu-Fano plots [9] can provide an efficient tool with which to analyze spectra within a two-channel model. The technique of Lu-Fano plots was initially developed in the framework of the multichannel quantum defect theory (MQDT) [10–13] and used for interpretation of experiments with electron-ion collisions or Rydberg atoms. Recently Lu-Fano plots were generalized to potentials with non-Coulomb and in particular R^{-n}, $n>2$ asymptotic behavior [14,15]. It was shown on numerical examples that two coupled vibrational progressions can be fitted by two generalized quantum defects and a coupling parameter. The latter can be extrapolated beyond a dissociation limit, yielding, for instance, accurate predictions for predissociation lifetimes [16]. The first aim of the present work is to apply the method of Lu-Fano plots to the analysis of an experimental molecular spectrum, and to check the accuracy of the data obtained. The second aim is to discuss whether the fitted parameters can be extrapolated beyond dissociation thresholds and provide information on quantities such as scattering cross sections.

The photoassociation spectra of Cs_2 molecules obtained by the Laboratoire Aimé Cotton group [6,17–19] exhibit many rovibrational progressions and several perturbations. The analysis of these progressions allowed for the determination of C_n parameters for the long-range interaction of atoms as well as for fitting molecular potential curves at smaller internuclear distances. The methods used were mainly Rydberg-Klein-Rees (RKR) procedures [18] or long-range analyses with the Le Roy–Bernstein formula. However some features in the spectra of $0_u^+(6S+6P_{1/2,3/2})$ symmetry remained unexplained, due to the coupling between the two $0_u^+(P_{1/2})$ and $0_u^+(P_{3/2})$ channels. A possible way of overcoming this difficulty was to solve the multichannel Schrödinger equation as was done, for example, in Refs. [14,16,20]. The main disadvantage of this approach is that one needs to know the interatomic potentials and coupling matrix elements for the Cs_2 dimer with great precision [14,21], well beyond the present achievements of accurate *ab initio* quantum chemistry calculations [22,23]. In practice, one proceeds [14,20,24] by trial and error through arbitrary small changes in the short distance potentials until the computed vibrational energy levels are in agreement with the experiment in a given energy range. Then, the fitted potential can be used to predict levels in another energy domain. This fitting procedure usually requires a lot of effort, especially in the present case where there are two coupled potentials and one R-dependent coupling term, and there is no unique solution.

However, small changes in the molecular potential by modifying the position of the repulsive wall result in a global shift of the vibrational progression. For highly excited levels this shift can be described by one parameter, similar to the quantum defect used in the analysis of Rydberg series for

electronic states. This analogy suggests the introduction of a generalized quantum defect theory for the analysis of the photoassociation spectra.

This was discussed in two recent papers [14,15], demonstrating the efficiency of the Lu-Fano method in analyzing the computed energy levels of the $0_u^+(6S+6P_{1/2,3/2})$ vibrational progressions in Cs_2 obtained from numerical two-channel calculations with a theoretical potential. The computed energies could indeed be represented by Lu-Fano plots and fitted by three parameters on a wide energy range. The availability of data [19] on the spectroscopy of the cesium molecule near the $6S+6P_{1/2}$ and $6S+6P_{3/2}$ limits now makes possible a direct application of the method to the interpretation of experimental spectra of Cs_2.

This article is organized as follows. In Sec. II we present experimental spectra and we discuss the difficulty of their interpretation within the usual Le Roy–Bernstein approach. In Sec. III we show that the Lu-Fano analysis provides a good interpretation. The derivation of Lu-Fano parameters is discussed, and we present a scaling law for the variation of the predissociation lifetimes as a function of detuning. In Sec. IV we discuss the possible extrapolation of the parameters over the $6S+6P_{3/2}$ dissociation limit to give information on scattering cross sections. Section V gives a discussion of trap loss measurements in the framework of the Lu-Fano analysis. Section VI is the conclusion.

II. EXPERIMENTAL SPECTRA AND THE LE ROY–BERNSTEIN APPROACH

In the photoassociation spectroscopy experiments, the cold atom source is provided by a Cs vapor loaded magneto-optical trap. Details of the experimental setup have been published in several previous articles (see, for instance, [17]). The photoassociation is achieved by continuously illuminating the cold Cs atoms with the beam of a Ti:sapphire laser pumped by an argon ion laser, red detuned compared to the $6S_{1/2}\rightarrow 6P_{1/2}$ or $6S_{1/2}\rightarrow 6P_{3/2}$ atomic transition; one has

$$2\mathrm{Cs}(6S,f=4)+h\nu_1 \rightarrow \mathrm{Cs}_2(\Omega_{u,g}6S+6P_{1/2\text{ or }3/2};v,J). \quad (1)$$

The frequency scale is calibrated using a Fabry-Perot interferometer, and the absorption lines of iodine [25]. The maximum available power of the laser beam is 650 mW focused in the trap with a waist of about 300 μm, corresponding to a maximum intensity of 450 W/cm^2. In the experiments, two kinds of detection are used for observing the photoassociation process. First we observe with a photodiode the fluorescence yield from the trap, which allows one to analyze the trap losses due to photoassociation and to obtain vibrational progressions with the observation of resonances. Second, we perform photoionization of the translationally cold Cs_2 molecules in Cs_2^+ ions, which are detected through a time of flight mass spectrometer. Ionization is made using a pulsed dye laser ($\lambda_2\sim 716$ nm, 7 ns duration) pumped by the second harmonic of a Nd-YAG (yttrium aluminum garnet) laser; it is a resonance enhanced multiphoton ionization (REMPI) process, using as an intermediate step vibrational levels of electronic molecular states correlated to the $6S_{1/2}+5D_{3/2,5/2}$ dissociation limits [6].

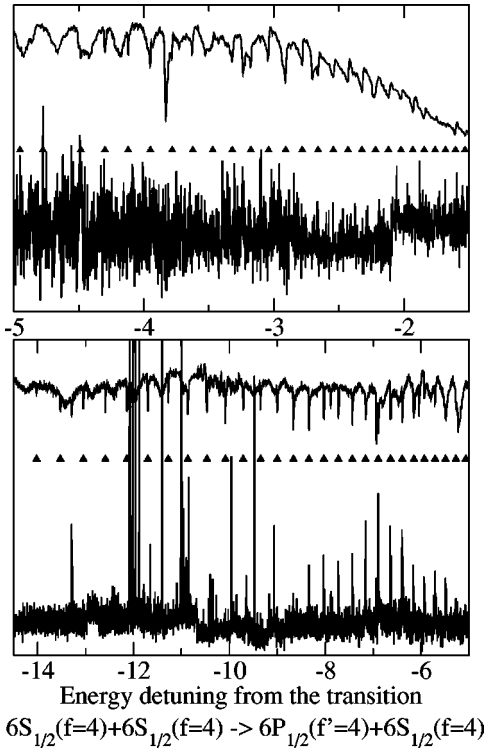

FIG. 1. The experimental spectrum of Cs_2 under the $6S+6P_{1/2}$ asymptote versus photoassociation laser frequency. The frequency laser is calibrated in cm^{-1} compared to the atomic transition $6S_{1/2}(f=4)+6S_{1/2}(f=4)\rightarrow 6S_{1/2}(f=4)+6P_{1/2}(f'=4)$. The upper line of both panels represents the fluorescence spectrum (arbitrary scale, see a calibrated spectrum in [19]); the lower line is the Cs_2^+ ion's number signal, which presents resonance in detuning between -15 cm^{-1} and -5 cm^{-1}. Several progressions are identified in the spectra. Triangles show positions of discrete 0_u^+ levels calculated using the Lu-Fano plot analysis: they are in excellent agreement with the measured levels (discrepancy less than 0.01 cm^{-1}). In contrast, the "standard" analysis using the Le Roy–Bernstein formula fails near the energy -5 cm^{-1} where a $6S+6P_{3/2}$ level perturbs the $6S+6P_{1/2}$ progression (Fig. 3); see for comparison the Fig. 4 of Ref. [19]. The discrepancy between energies predicted from the Le Roy–Bernstein analysis and the measured ones can reach 0.1 cm^{-1}.

Figures 1 and 2 show the observed spectra of the vibrational progression below the dissociation limits $6S+6P_{1/2}$ and $6S+6P_{3/2}$, respectively. The energy detuning is calibrated relative to the transitions from $6S_{1/2}(f=4)$ to $6P_{1/2}(f'=4)$ and from $6S_{1/2}(f=4)$ to $6P_{3/2}(f'=5)$, respectively; however, here and in the following discussion we will omit the notation for hyperfine quantum numbers $f,f'=4,5$ since they do not enter explicitly in our formulas. In a previous paper [19], the vibrational progressions have been identified. We can note that in previous work all the progressions corresponding to allowed photoassociation transitions have been observed in the spectra, the identification relying upon the Le Roy–Bernstein approach and the hyperfine width of the resonances. In the present paper we focus our

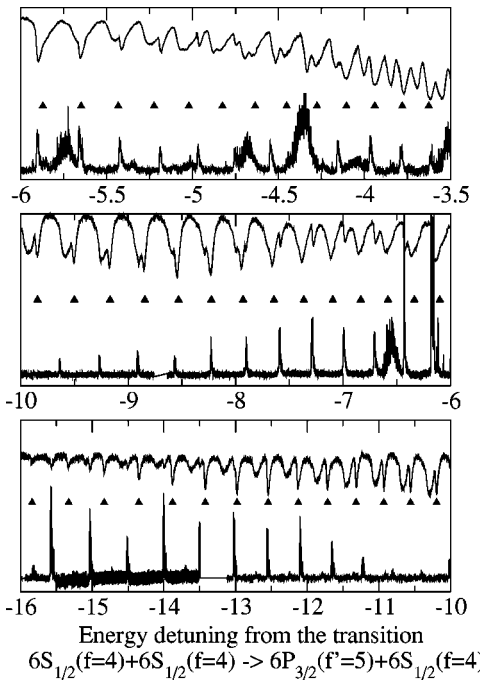

FIG. 2. Same as Fig. 1, but for the energy region just under the $6S+6P_{3/2}$ asymptote. Triangles show positions of discrete 0_u^+ levels. Such levels are present only in the trap-loss spectrum. The frequency laser is calibrated in cm^{-1} relative to the atomic transition $6S_{1/2}(f=4)+6S_{1/2}(f=4)\rightarrow 6S_{1/2}(f=4)+6P_{3/2}(f'=5)$.

effort on the vibrational progressions corresponding to the $0_u^+(6S+6P_{1/2})$ and to $0_u^+(6S+6P_{3/2})$ states.

The Le Roy–Bernstein formula [7] allows the analysis the two vibrational progressions $E_1(v)$ and $E_2(v)$ when they are assumed unperturbed. Indexes 1 and 2 correspond to $0_u^+(6S+6P_{1/2})$ and to $0_u^+(6S+6P_{3/2})$ progressions, respectively. Both progressions near the dissociation limits can be described by the analytical Le Roy–Bernstein formula [7],

$$E_i(v)=D_i-[H_i(v_{D_i}-v)]^6. \tag{2}$$

In Eq. (2) the parameter D_i is the dissociation limit for channel i and the v_{D_i} parameter is linked to the phase δ_i at the dissociation limit by $v_{D_i}=\pi\delta_i$ and can be interpreted as the total (not necessary integer) number of bound levels in the potential i. The H_i parameter is related to the C_3 coefficient of the long-range 0_u^+ potential [7]. In fact, the first order asymptotic behavior of the $0_u^+(6S+6P_{1/2})$ and $0_u^+(6S+6P_{3/2})$ curves varies, respectively, as $C_3(P_{1/2})/R^3=-4/3(C_3^{(d)}/R^3)$ and $C_3(P_{3/2})/R^3=-5/3(C_3^{(d)}/R^3)$ with $C_3^{(d)}=\langle 6s|d_z|6p\rangle^2$ [26–28]. We apply the three-parameter relation (2) to fit the experimental 0_u^+ vibrational progression converging to the $6S+6P_{3/2}$ limit [17]. We resolve about 60 vibrational lines between 40 and 2.5 cm^{-1} from the D_2 dissociation limit. These lines are only present in the fluorescence spectrum. No resonance corresponding to the $0_u^+(6S+6P_{3/2})$ excitation is observed in the ion spectrum, indicating that no formation of cold molecules is obtained in this channel. We find a value for the $C_3^{(d)}$ coefficient of 9.85 ± 0.15 a.u. This determination is compatible with the value 10.035 a.u. obtained from the accurate experimental radiative lifetime [29]. The transition dipole moment matrix element and the $C_3^{(d)}$ coefficient are linked by the relation: $\tau(P_{3/2})=3\pi\varepsilon_0\hbar c^3/\omega^3 C_3^{(d)}$. There is only a weak discrepancy of about 3% between both values, mostly linked to different approximations in the Le Roy–Bernstein approach: the higher order multipolar terms $(C_6/R^6, C_8/R^8, \ldots)$ at short internuclear distance, the hyperfine broadening of the spectra line and the retardation effects at long internuclear distance near the dissociation limit. Typically, at 10 cm^{-1} detuning, the C_6/R^6 term is introducing a 10^{-2} cm^{-1} correction while the hyperfine splitting should be considered at low detuning. A more detailed analysis as in [1–5] would lead to better agreement and a more accurate determination of the lifetime, but is beyond the scope of the present work.

Concerning the $0_u^+(6S+6P_{1/2})$ progression converging to the $6S+6P_{1/2}$ limit, we observe 76 lines either in the fluorescence or in the ion spectra, at detunings between 14 and 0.5 cm^{-1} from the D_1 dissociation limit. This channel does lead to the formation of ground-state cold molecules due to internal coupling between both 0_u^+ states as analyzed in Ref. [24]. If we try to apply the same Le Roy–Bernstein analysis as for the $0_u^+(6S+6P_{3/2})$ progression, the interpolation procedure fails for $0_u^+(6S+6P_{1/2})$: different groups of levels lead to very different values of the set of three parameters.

To interpret the failure of the Le Roy–Bernstein approach in the analysis of the latter data, and/or to verify the precision and the validity of the interpolation in the first example, we invert the relation (2),

$$v_{fit}=v_{D_i}-\frac{[D_i-E]^{1/6}}{H_i}=v_{D_i}-\nu_i. \tag{3}$$

Then, for a given experimental energy E we can recalculate the value (no longer an integer) of v_{fit} as a function of the parameters v_{D_i}, D_i, and H_i found by fitting to 74 levels. We plot the quantity $(v-v_{fit})$ as a function of v (see Fig. 3). We see that the Le Roy–Bernstein approach is well adapted for the $0_u^+(6S+6P_{3/2})$ progression because the dispersion of the corresponding points (white triangles in Fig. 3) around zero is small. This is not the case for the $0_u^+(6S+6P_{1/2})$ progression where we observe a large dispersion of the corresponding points (black circles in Fig. 3). The reason for this lies in the coupling between the two 0_u^+ channels and more precisely here, in the presence of one level of the $0_u^+(6S+6P_{3/2})$ progression at an energy below the asymptotic limit $(6S_{1/2}+6P_{1/2})$ in the part of the spectrum experimentally measured. There are a lot of other $0_u^+(6S_{1/2}+6P_{3/2})$ levels below this energy region perturbing the $0_u^+(6S+6P_{1/2})$ progression, which are not accessible in the present experiment. However, the plotted deviation looks very similar to a Lu-Fano plot, and we shall explore this approach in the following section.

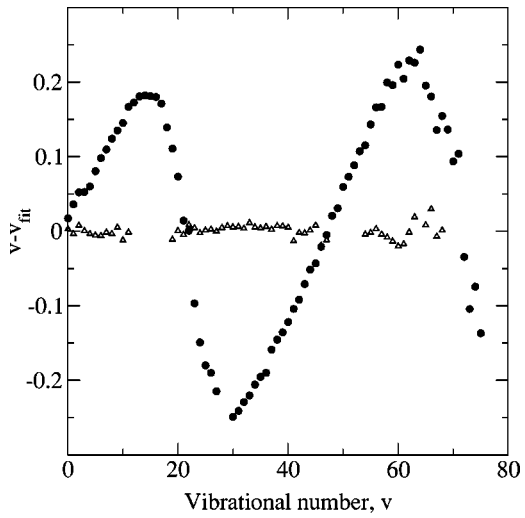

FIG. 3. Discussion of the validity of a Le Roy–Bernstein law to fit the $0_u^+(6S+6P_{1/2})$ progression (black circles) and $0_u^+(6S+6P_{3/2})$ progression (white triangles). Considering the levels observed below both dissociation limits, with arbitrary numbering v (see text) from the lower level, the quantity $(v-v_{fit})$ is plotted.

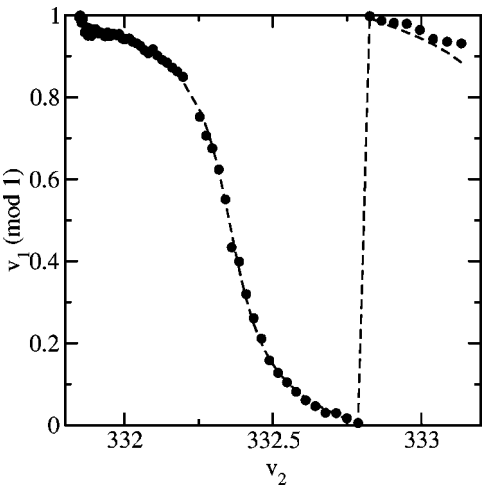

FIG. 4. The Lu-Fano plot of the experimental $0_u^+(6S+6P)$ spectrum. One $0_u^+(6S+6P_{3/2})$ vibrational level perturbs the $0_u^+(6S+6P_{1/2})$ progression. See Fig. 3 for comparison.

III. LU-FANO PARAMETERS AND THEORETICAL PREDICTIONS

A. Lu-Fano plot

Since the potentials are unknown at short distances and since the experiment is observing only the upper vibrational levels, we may start counting bound levels from the lower level observed experimentally: a change of v_{D_i} by unity adds one extra bound level, and the Le Roy–Bernstein law (2) depends only on the difference $v_{D_i}-v=\nu_i$ and not on the absolute numbering.

The construction of a Lu-Fano plot from the experimental data is straightforward: for each experimental energy E of a 0_u^+ discrete level two values $\nu_1(E)$ and $\nu_2(E)$ are determined from the inverse relation (3), which rely on the choice for the parameters D_i, H_i, and v_{D_i}. The value $\nu_2(E)$ is plotted as the abscissa while the value $\nu_1(E)$ modulo 1 is plotted as the ordinate. The result is shown in Fig. 4. This figure also shows a presence of one perturber similarly as the graph in Fig. 3 does. But a difference between the two figures is that the graphical representation of Fig. 4 allows the extraction of information about the coupling between the two progressions. Since the Lu-Fano plot is extremely sensitive to parameters D_i and H_i (assuming a large number of levels as in our case), these parameters can be themselves adjusted: the criterion is that all experimental energies should be located on a curve determined by the Lu-Fano formula, depending upon three parameters according to

$$\tan[\pi(\nu_1+\tilde{\mu}_1)]\tan[\pi(\nu_2+\tilde{\mu}_2)]=\xi^2. \tag{4}$$

The parameters are determined by fitting on a small number of points (two usually being sufficient), and then checking that the maximum number of levels, out of the 74 observed ones, should be well represented by Eq. (4). Such a fit can be done only if H_i and D_i are well defined. From the best fit, the parameter H_1 is found to be 0.00935 ($\pm 1\%$) $\mathrm{cm}^{-1/6}$ (0.001204 a.u.). It corresponds to the value -13.25 ($\pm 6\%$) a.u. of the coefficient $C_3(P_{1/2})$ for long-range behavior C_3/R^3 of the $0_u^+(6S+6P_{1/2})$ potential. This yields $C_3^{(d)}=9.94$ ($\pm 6\%$) a.u., in agreement with the value determined in Sec. II from the Le Roy–Bernstein fit to the $0_u^+(P_{3/2})$ progression below the $6s+6P_{3/2}$ dissociation limit.

Since there is only one level of the $0_u^+(6S+6P_{3/2})$ progression in the energy range of the experiments, the parameter H_2 cannot be determined precisely from this set of data. We used in the fit $H_2=0.0086$ $\mathrm{cm}^{-1/6}$ corresponding to the coefficient $C_3(P_{3/2})=-16.78$ a.u., obtained from the accurate experimental radiative lifetime [29]. A correct fit would require a spectrum spanning a larger energy range with several levels from this progression.

Once the fitted parameters $\tilde{\mu}_1$, $\tilde{\mu}_2$, and ξ have been determined from some observed values, the energies of other bound levels can be recomputed from Eq. (4) as follows. The energy E_{fit}^v of any bound level satisfies Eq. (4), where quantities $\nu_i(E_{fit}^v)$ depend on E_{fit}^v according to Eq. (3). Thus, Eq. (4) can be considered as a nonlinear equation with respect to E_{fit}^v which enters twice in the equation. Each solution of the equation gives a bound level. The comparison between the fitted spectrum and the observed one is given by the triangles in Fig. 1. The agreement is now excellent, the discrepancy in the positions not exceeding 0.01 cm^{-1}, while for most levels it is ten times smaller. In contrast, when we previously tried a fit by the Le Roy–Bernstein law, the disagreement between observed and measured levels was as strong as 0.1 cm^{-1} at the maxima of the deviation in Fig. 3.

B. Lu-Fano parameters in the vicinity of the $P_{1/2}$ asymptote

Having constructed the Lu-Fano plot, we have obtained three parameters $\tilde{\mu}_1$, $\tilde{\mu}_2$, and ξ, which can be interpreted as two generalized quantum defects and one coupling parameter

[14,16]. In the present work we employ the formulation introduced by Eissner *et al.* (see Refs. [30,31]),

$$\tan[\pi(\nu_1+\tilde{\mu}_1)]\tan[\pi(\nu_2+\tilde{\mu}_2)]=\xi^2. \tag{5}$$

Fitting the analytical dependence $\nu_1(\nu_2)$ obtained from Eq. (4) to the experimental data, we determined the parameters $\tilde{\mu}_1$, $\tilde{\mu}_2$, and ξ,

$$\begin{aligned}\tilde{\mu}_1&=0.0155,\\ \tilde{\mu}_2&=0.643,\\ \xi&=0.521.\end{aligned} \tag{6}$$

As was shown in Refs. [14–16,32,33] these parameters depend weakly on energy and can be used for the calculation of various observables: positions of spectral lines in the discrete spectrum, widths of resonances in the predissociation energy domain, and scattering cross sections. Owing to a weak energy dependence, the calculations can be extended to the energy regions experimentally inaccessible. Hopefully, we can correct the values of $\tilde{\mu}_2$ and ξ for the energies just under the $P_{3/2}$ dissociation limit, for which experimental observations exist [19].

C. Lu-Fano parameters in the vicinity of the $P_{3/2}$ asymptote: Predissociation effects

Predissociation widths in the spectrum below the $6S+6P_{3/2}$ threshold are linked to the parameter ξ [16] and to the level spacing $\Delta E=dE/dv_2$ by

$$\Gamma(v_2)=\frac{2}{\pi}\xi^2\Delta E. \tag{7}$$

The positions E_{v_2} of the resonances are linked to the quantum defect $\tilde{\mu}_2$ by the Le Roy–Bernstein formula of Eq. (2). Thus, the two parameters can be determined from the experimental spectrum on Fig. 2. From the analysis of positions of 38 resonances at detuning between -16 cm^{-1} and -4 cm^{-1} we found that the best fit to Eq. (2) is obtained for

$$\begin{aligned}H_2&=0.0011112 \text{ a.u.},\\ v_{D_2}&=332.63.\end{aligned} \tag{8}$$

We discuss the accuracy of the determination of these parameters in Sec. V. The limitation in the analysis of widths is due to the presence of vibrational progressions corresponding to other symmetries, and to the effect of hyperfine coupling which is not considered in the present two-state model. For the analysis of widths we took a smaller number, 15, of resonances in the region where the 0_u^+ levels do not overlap with vibrational levels of other progressions. Figure 5 shows the result of the analysis as quantity $\xi=\sqrt{\pi\Gamma/(2\Delta E)}$. We obtained $\xi=0.44$, a value 16% smaller than in Eq. (6). Thus, parameters $\tilde{\mu}_i$ and ξ are

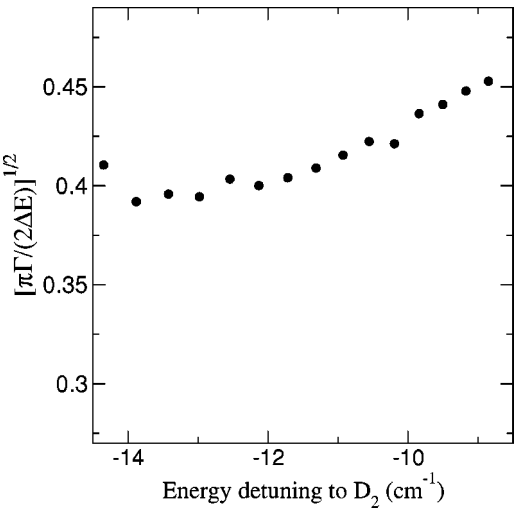

FIG. 5. Analysis of widths of several experimental 0_u^+ resonances. The presented quantity $\sqrt{\pi\Gamma/(2\Delta E)}=\xi$ should be constant according to our theoretical model. The existing deviation from a constant is due to the hyperfine structure.

$$\begin{aligned}\tilde{\mu}_1&=0.0155,\\ \tilde{\mu}_2&=0.63,\\ \xi&=0.44.\end{aligned} \tag{9}$$

The value $\xi=0.44$ was estimated with an uncertainty of 10%, due to the uncertainty on the widths which could be modified by hyperfine broadening (see Sec. V). The fact that two values $\xi=0.52$ and 0.44 are obtained from different energy regions indicates that the parameter ξ is varying with the energy. The energy gap between two regions is about 600 cm^{-1}; this variation can be considered as slow, in the spirit of generalized quantum defect theory. In previous theoretical work [14,16], the predissociation lifetimes of the $0_u^+(P_{3/2})$ vibrational levels above the $P_{1/2}$ limit have been computed using the *ab initio* potential curves of Spies and Meyer [22] and numerical calculations. Theoretical values for the quantum defects and couplings were then

$$\begin{aligned}\tilde{\mu}_1^{the}&=0.048,\\ \tilde{\mu}_2^{the}&=-0.096,\\ \xi^{the}&=0.1.\end{aligned} \tag{10}$$

Parameters $\tilde{\mu}_1^{the}$ and $\tilde{\mu}_2^{the}$ depend strongly on the potential curves used in the calculation. The present accuracy of the Cs_2 potentials does not allow a precise theoretical calculation of these parameters and is the reason why theoretical values are so different from the parameters extracted from the experiment.

The coupling parameter ξ reflects the strength of the interaction between the two progressions and was found markedly dependent upon the value of the molecular spin-orbit coupling in the region of the pseudocrossing between the two curves. When the atomic value is chosen, the crossing can be

considered as nearly adiabatic and there is little interaction between the two vibrational progressions, and $\xi=0.03$. The value $\xi^{the}=0.1$ above was computed from the R-dependent molecular spin-orbit coupling computed in Ref. [22], corresponding to a strong decrease of the interaction in the region of the pseudocrossing. The present fit yields an even larger value $\xi=0.44$ of the parameter, which would indicate an even weaker value of the molecular spin-orbit coupling. In any case, the predissociation lifetimes are larger than in previous work [16]. In a range of 100 cm^{-1} below the D_2 dissociation limit, the lifetimes $\tau(E_{v_2})$ could be fitted by an analytical formula,

$$\frac{1}{\tau(E_{v_2})}=\Gamma(v_2)=\frac{1}{\alpha}(D_2-E_{v_2})^{5/6}. \tag{11}$$

The coefficient α is related to ξ by

$$\alpha=\frac{\pi}{12\xi^2 H_2}. \tag{12}$$

This formula is easily obtained from Eqs. (2), (7), and (11).

For the previous theoretical value $\xi=0.1$ [16], $\alpha=23\,600$ a.u. or 16.1 $(cm^{-1})^{5/6}$ μs. For the present value $\xi=0.44$, fitted to the experiment, $\alpha=1220$ a.u. or 830 $(cm^{-1})^{5/6}$ ps.

This scaling law, predicting a decrease of the lifetimes as a function of detuning, corresponds to a model where the lifetime is proportional to the classical vibration period of the predissociated level, since the predissociation is taking place in the short region with a transition probability that can be assumed constant. More complex situations can occur. Previous calculations have shown a minimum of the lifetimes at 100 cm^{-1} detuning below the $P_{3/2}$ asymptote, followed by an increase at larger detuning. This nonuniform dependence of lifetimes reflects a nontrivial behavior of Franck-Condon overlaps between continuum $P_{1/2}$ vibrational wave functions and bound $P_{3/2}$ wave functions. The minimum value for lifetimes was found to be $\approx$350 ps. The present calculation based on the parameters extracted from the experiment gives a value 18 ps for the same energy detuning. In the region where the experiments of the present paper are performed, at detunings $\sim$10 cm^{-1}, the lifetime is $\sim$120 ps. The drastic reduction at larger detunings, found in the previous work, is to be checked by further experiments.

IV. EXTRAPOLATING ABOVE THE $P_{3/2}$ ASYMPTOTE: SCATTERING CROSS SECTIONS

Having the three MQDT parameters, the cross section for the collision

$$Cs(6S)+Cs(0_u^+ 6P_{3/2})\rightarrow Cs(6S)+Cs(0_u^+ 6P_{1/2}) \tag{13}$$

can also be calculated.

In order to calculate the cross section one additional intermediate step should be made: namely, the connection between the parameters $\tilde{\mu}_1$, $\tilde{\mu}_2$, and ξ and the S matrix. It can be done in a spirit proposed by Burke *et al.* [32] and by Mies and Raoult [33].

The only difficulty to solve is how to connect the reaction matrix K (R in Ref. [33]) used in Refs. [32,33] and the parameters $\tilde{\mu}_1$, $\tilde{\mu}_2$, and ξ of the present work. For this we used an approach quite similar to the one proposed by Giusti-Suzor and Fano [30].

The reaction matrix K is closely linked to another formulation of the Lu-Fano plots [11,12]:

$$\begin{aligned}&\sin[\pi(\nu_1+\mu_1)]\sin[\pi(\nu_2+\mu_2)]\\&\quad+\tan^2\theta\sin[\pi(\nu_1+\mu_2)]\sin[\pi(\nu_2+\mu_1)]\\&\quad=0.\end{aligned} \tag{14}$$

Equations (4) and (14) represent the same dependence $\nu_1(\nu_2)$ but with different sets of constants, $\tilde{\mu}_1$, $\tilde{\mu}_2$, and ξ or μ_1, μ_2, and θ and the connection between them can be established as follows.

Equation (14) can be rewritten as

$$\begin{aligned}&[\tan(\pi\nu_1)+\tan(\pi\mu_1)][\tan(\pi\nu_2)+\tan(\pi\mu_2)]\\&\quad+\tan^2\theta[\tan(\pi\nu_1)+\tan(\pi\mu_2)]\\&\quad\times[\tan(\pi\nu_2)+\tan(\pi\mu_1)]=0.\end{aligned} \tag{15}$$

We solve both Eqs. (4) and (15) with respect to $\tan(\pi\nu_1)$. Each solution has the form

$$\tan(\pi\nu_1)=A+\frac{B}{\tan(\pi\nu_2)+C}. \tag{16}$$

Equating the coefficients A, B, and C for both solutions we obtain three equations,

$$\begin{aligned}&\frac{\tan(\pi\mu_1)+\tan(\pi\mu_2)\tan^2\theta}{1+\tan^2\theta}=\frac{\tan(\pi\tilde{\mu}_1)+\tan(\pi\tilde{\mu}_2)\xi^2}{1-\xi^2\tan(\pi\tilde{\mu}_1)\tan(\pi\tilde{\mu}_2)},\\&-\frac{\tan(\pi\mu_1)\tan(\pi\mu_2)(1+\tan^2\theta)}{1+\tan^2\theta}\\&\quad=\frac{\xi^2-\tan(\pi\tilde{\mu}_1)\tan(\pi\tilde{\mu}_2)}{1-\xi^2\tan(\pi\tilde{\mu}_1)\tan(\pi\tilde{\mu}_2)},\\&-\frac{\tan(\pi\mu_2)+\tan(\pi\mu_1)\tan^2\theta}{1+\tan^2\theta}=\frac{\xi^2\tan(\pi\tilde{\mu}_1)+\tan(\pi\tilde{\mu}_2)}{1-\xi^2\tan(\pi\tilde{\mu}_1)\tan(\pi\tilde{\mu}_2)}.\end{aligned} \tag{17}$$

These nonlinear equations link the parameters $\tilde{\mu}_1$, $\tilde{\mu}_2$, and ξ and μ_1, μ_2, and θ. We have numerical values for one set of parameters and another set can be easily found by existing numerical methods. We used the MATHEMATICA package to solve the nonlinear system (17). For parameters of Eq. (9) we obtained

$$\mu_1=0.0345,$$

$$\mu_2 = -0.389,$$
$$\theta = 0.431. \tag{18}$$

The matrix K is calculated as [11,12]

$$K = U \tan(\pi \underline{\mu}) U^T, \tag{19}$$

where μ is a diagonal matrix with diagonal elements $\tan(\pi\mu_1)$ and $\tan(\pi\mu_2)$, and U is a matrix with elements:

$$U_{1,1} = U_{2,2} = \cos\theta,$$
$$U_{1,2} = -U_{2,1} = \sin\theta. \tag{20}$$

The S matrix for the region above the second dissociation limit $6S+6P_{3/2}$ is calculated as [32,33]

$$S = e^{i\eta} \frac{1+iK}{1-iK} e^{i\eta}. \tag{21}$$

Diagonal elements η_1 and η_2 of the diagonal matrix η describe the asymptotic phase shift (or quantum defect) of used reference functions [11,12] for unperturbed progressions with respect to the asymptotic sine function [32]. In the present case the unperturbed vibrational progressions are chosen in a way which implies that there should be a vibrational level just at the dissociation limits. It corresponds to $\eta = \pi/2$.

In Eq. (20) we have not included terms describing non-WKB effects near threshold [32–35]. This approximation is justified by the fact that these corrections have an important influence only for the very last levels close to the thresholds D_1 or D_2. In the present results, we are not close to the D_2 threshold, and the difference $v_{D1} - v$ is larger than 100.

The total partial cross section corresponding to "s" scattering for the transition $i \rightarrow j$ is calculated as [36]

$$\sigma^s_{ji} = \frac{\pi}{k_i^2} [|S_{ji}|^2 - 2\delta_{ji} \,\mathrm{Re}\, S_{ii} + \delta_{ji}]. \tag{22}$$

Performing calculations using Eqs. (17), (19), (20), and (22) for parameters of Eq. (18), the cross sections can be written in the form (in atomic units)

$$\sigma^s_{11}(E) = \frac{1.14\times10^{-4}}{E - D_1},$$
$$\sigma^s_{21}(E) = \frac{2.21\times10^{-5}}{E - D_1},$$
$$\sigma^s_{12}(E) = \frac{2.21\times10^{-5}}{E - D_2}, \tag{23}$$
$$\sigma^s_{22}(E) = \frac{2.16\times10^{-5}}{E - D_2}.$$

Figure 6 shows the cross sections as functions of the energy above the $6S+6P_{3/2}$ dissociation limit. The present calculations are limited to s-wave scattering, and to transitions within the 0_u^+ symmetry.

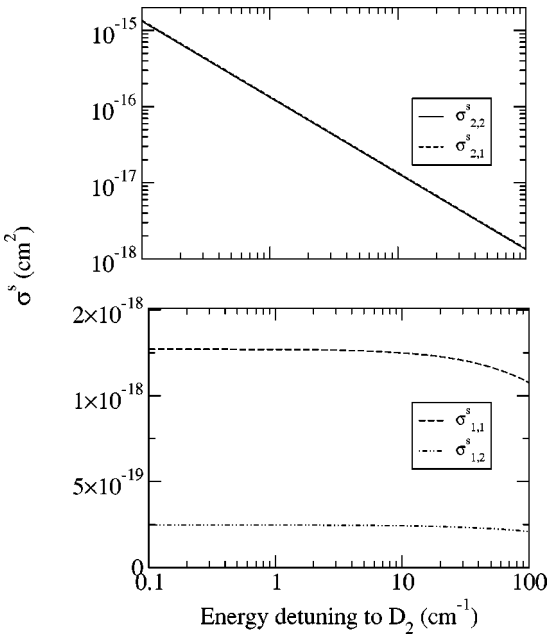

FIG. 6. Partial cross sections for s-wave scattering of Cs($6S$) + Cs($6P_{1/2,3/2}$) computed in a two-state model considering spin-orbit coupling in the 0_u^+ symmetry for the energy domain above the ($6S+6P_{3/2}$) limit. Lines for $\sigma_{1,1}$ and $\sigma_{1,2}$ almost coincide.

The total cross sections for fine-structure transitions

$$\mathrm{Cs}(6S) + \mathrm{Cs}(6P_{3/2}) \rightarrow \mathrm{Cs}(6S) + \mathrm{Cs}(6P_{1/2}) \tag{24}$$

have been discussed theoretically by Dashevskaya and Nikitin [37], who demonstrated the importance of the 0_u^+ coupling mechanism, and by Julienne and Vigué [27], who showed that this mechanism was dominant. The latter authors showed that the probability is oscillating as a function of the partial wave, the average value being nearly constant as a function of energy. The computed values depend markedly on the choice for the spin-orbit coupling V_{SO} in the region of the pseudocrossing between the two 0_u^+ potential curves: for $V_{SO} = 150$ cm^{-1}, the authors find a probability varying from 0.41 to 0.43 as the energy E/kB decreases from 300 K to 1 mK ; for $V_{SO} = 188$ cm^{-1}, the probability is varying from 0.24 to 0.29. In the lack of a rotational analysis, the probability that we find can be considered as an average value for a few partial waves rather than an s-wave scattering cross section. It is then meaningful to compare our probability to their calculations, based on *ab initio* potentials. The present calculations, based on fitted parameters, yields a somewhat larger probability of 0.54. This probability is linked to the parameter ξ by $P = 2.8\xi^2$. Direct comparison with cold collision experiments cannot be implemented, as Fioretti *et al.* [38,39] have demonstrated the importance of hyperfine coupling at very low collision energies, which is not included in the present model. However, the validity of a two-state model can be checked from trap-loss measurements below the ($6S+6P_{3/2}$) asymptote as described below.

V. DISCUSSION OF THE VALIDITY OF A TWO-STATE MODEL: INTERPRETATION OF TRAP-LOSS MEASUREMENTS BELOW THE $P_{3/2}$ LIMIT

To obtain the cross section for the energy domain between the two dissociation limits we use the same equations (20) and (22). The only difference is the matrix K used for calculation of the S matrix. For this energy domain only the D_1 limit is open for dissociation. In this situation instead of K one uses the matrix K^{phys} [11]. The expression for K^{phys} is very simple in our case since there is only one closed channel and one open channel. The K^{phys} matrix becomes a scalar value:

$$K^{phys}=K_{1,1}-\frac{K_{1,2}^2}{K_{2,2}+\tan[\pi\nu_2(E)]}, \tag{25}$$

where $\nu_2(E)$ is a continuous function of energy from Eq. (3). The factor $\tan[\pi\nu_2(E)]$ accounts for a contribution from the predissociation of quasidiscrete $0_u^+(6S+6P_{3/2})$ levels to the total cross section $\sigma_{1,1}$ for energies between the two limits. We can compare to experiment in a model where the photoassociated molecule is decaying mainly through predissociation according to Eq. (24).

Figure 7 shows the comparison between experimental and theoretical cross sections. The experimental data are the trap fluorescence signal [19]. This curve is arbitrary scaled to fit the theoretical cross-section in amplitude. Positions and widths of resonances are in a fairly good agreement for many predissociated levels of the $0_u^+(6S+6P)$ symmetry. One may wonder why for several resonances between -8 and -5 cm^{-1} the agreement for positions is not good. For this energy region the 0_u^+ resonances are overlapped with two other vibrational progressions (1_g and 0_g^-). The interplay of relative contributions to the total cross section from the three progressions gives a somewhat incorrect impression about positions of separate resonances. For a smaller and a larger detuning, where the 0_u^+ progression is separated from the two other progressions, the agreement is evident.

At this point we make some notes about the accuracy of present calculations. As one can see, positions of calculated resonances are in a very good agreement with experiment: for 38 resonances the accumulated difference between calculation and experiment is less than 5% of $(E_{v_2+1}-E_{v_2})$. This makes the relative error in determination of H_2 of order $0.05/38\approx 0.0013$. $H_2=0.001\,111\,2\pm 0.000\,001\,5$ a.u. or $0.008\,63\pm 0.000\,01$ cm$^{-1/6}$. Thus, the $C_3(P_{3/2})$ coefficient is determined as 16.85 ± 0.07 a.u. giving $C_3^{(d)}=10.11\pm 0.4\%$. The accuracy in determination of widths is much worse. We estimate the accuracy of the fit for ξ as about 10% which makes the error in calculated widths of order 20%. The accuracy of the cross section is determined by the same error since it is controlled by ξ^2.

At low detunings, the two-state model is not valid and the hyperfine broadening becomes dominant. One way of checking the validity of the two-state model is to verify the validity of relation (7) linking the width of the resonances to the spacing between neighboring levels. This is represented by Fig. 5. One can see that although $\xi=\sqrt{\pi\Gamma/(2\Delta E)}$ is a constant around 0.44, it has a small increasing trend for the in direction of smaller detunings, indicating the fact that the hyperfine structure is not completely negligible in this region. For smaller detunings the hyperfine structure becomes dominant as is seen in Fig. 7.

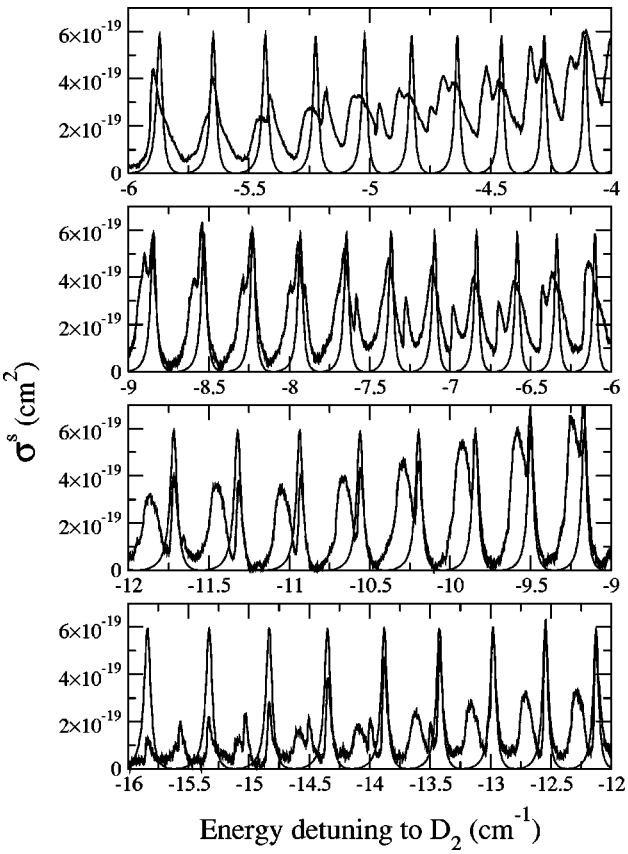

FIG. 7. Calculated (gray line) and experimental (dark black line) cross sections under the $6S+6P_{3/2}$ dissociation limit. The experimental curve is the trap fluorescence signal, arbitrarily scaled in amplitude to fit the theoretical curve. Note the variation in the horizontal scale from the upper figure to the lower one. The calculated cross section takes into account only the trap loss signal due to channel coupling in the $0_u^+(6S+6P)$ symmetry. In the experimental spectrum other vibrational progressions (1_g and 0_g^-) are present.

To obtain the probability 0.28, found by Julienne and Vigué using *ab initio* potential curves, ξ should be about 0.31. Future experimental data will hopefully answer the question whether the larger value for the fine structure probability in our estimation is realistic for the region above the $6S+6P_{3/2}$ limit, where there is no experimental information at the present time. For a full comparison, the variation of the parameter ξ with the rotational number should also be fitted.

VI. CONCLUSION

In conclusion several remarks are to be mentioned. We presented experimental data for photoassociation spectra obtained both by trap-loss measurements and molecular ion detection, where the two progressions of the $0_u^+(6S+6P)$ symmetry were identified. We have shown that the data of

the $0_u^+(6S+6P_{1/2})$ progression could not be fitted by the Le Roy-Bernstein formula in a region where they are perturbed by a level of the $0_u^+(6S+6P_{3/2})$ progression. In contrast, we have shown that the method of Lu-Fano plots could be successfully applied yielding a good interpretation. We have demonstrated that the method is very efficient and accurate for the extraction of parameters of diatomic interaction from experimental data in the case of two-coupled channels: a large number of level positions can be fitted by a three-parameter formula involving two generalized quantum defects and a coupling parameter estimated here as 0.44. Future work would benefit from experimental spectra extending on a larger energy region where several resonances are observed. In the present work, we were able to determine the $C_3^{(d)}$ coefficient with good accuracy, leading to the value $C_3^{(d)}=10.11\pm0.4\%$ (fit under the $6S+6P_{3/2}$ limit). Better accuracy could be obtained with a more accurate fit involving other terms in the multipole expansion.

Considering the spectrum below the $P_{3/2}$ limit, we have extracted Lu-Fano parameters from the positions and widths of the predissociated levels. Employing the Lu-Fano plot together with MQDT we were able not only to describe the observed features in the spectrum, but also to calculate different observables in energy domains where no experimental data were available. We have predicted a simple law for the variation of the lifetime as a function of detuning.

The cross section of the reaction $\mathrm{Cs}(6S)+\mathrm{Cs}(6P_i)\leftrightarrow\mathrm{Cs}(6S)+\mathrm{Cs}(6P_j)$ was estimated using parameters extracted from the experimental molecular spectrum. Within a two-state model, the probability is found to be 0.54, while the existing estimation of Julienne and Vigué for the average probability at 1 mK is 0.41 or 0.24 according to the choice of the coupling. Previous work [21] had stressed the fact that being very sensitive to the accuracy of short-range potentials, the fine-structure transition probability was a quantity difficult to estimate by theoretical calculations. Here we propose a method to obtain information by fitting the experimental bound spectra. The limitation of the present estimation relies on the presence of other vibrational progressions and on hyperfine broadening: the validity of a two-state model, where hyperfine structure effects are not included, was discussed by comparing the theoretical spectrum with the experimental trap-loss spectrum below the $6S+6P_{3/2}$ dissociation limit, suggesting that hyperfine broadening can be neglected in the detuning region ($-14\ \mathrm{cm}^{-1}$, $10\ \mathrm{cm}^{-1}$) where the present fit was performed.

Future work fitting experimental data at larger red detunings, where hyperfine coupling can safely be neglected, will possibly confirm the large value of the fine-structure transition probability found here. It would be very interesting to include rotation effects in the analysis in order to give information on the partial-wave dependence of the probability, and to compare with direct measurements of the total cross sections for cold cesium collisions.

ACKNOWLEDGMENTS

Discussions with Olivier Dulieu are gratefully acknowledged. V. Kokoouline thanks Chris Greene for many useful discussions and acknowledges support from a National Science Foundation grant.

[1] W. I. McAlexander, E. R. I. Abraham, N. W. M. Ritchie, C. J. Williams, H. T. C. Stoof, and R. G. Hulet, Phys. Rev. A **51**, R871 (1995).
[2] J. R. Gardner, R. A. Cline, J. D. Miller, D. J. Heinzen, H. M. J. M. Boesten, and B. J. Verhaar, Phys. Rev. Lett. **74**, 3764 (1995).
[3] W. I. McAlexander, E. R. I. Abraham, and R. G. Hulet, Phys. Rev. A **54**, R5 (1996).
[4] K. M. Jones, P. S. Julienne, P. D. Lett, W. D. Phillips, E. Tiesinga, and C. J. Williams, Europhys. Lett. **35**, 85 (1996).
[5] H. Wang, J. Li, X. T. Wang, C. J. Williams, P. L. Gould, and W. C. Stwalley, Phys. Rev. A **55**, R1569 (1997).
[6] A. Fioretti, D. Comparat, A. Crubellier, O. Dulieu, F. Masnou-Seeuws, and P. Pillet, Phys. Rev. Lett. **80**, 4402 (1998).
[7] R. J. Le Roy and R. B. Bernstein, J. Chem. Phys. **52**, 3869 (1970).
[8] G. Zinner, T. Binnewies, F. Riehle, and E. Tiemann, Phys. Rev. Lett. **85**, 2292 (2000).
[9] K. T. Lu and U. Fano, Phys. Rev. A **2**, 81 (1970).
[10] M. J. Seaton, Rep. Prog. Phys. **46**, 167 (1994).
[11] C. H. Greene and Ch. Jungen, Adv. At. Mol. Phys. **21**, 51 (1985).
[12] M. Aymar, C. H. Greene, and E. Luc-Koenig, Rev. Mod. Phys. **68**, 1015 (1999).
[13] Ch. Jungen, *Molecular Applications of Quantum Defect Theory* (Institute of Physics, Bristol, 1996).
[14] V. Kokoouline, O. Dulieu, and F. Masnou-Seeuws, Phys. Rev. A **62**, 022504 (2000).
[15] V. Ostrovsky, V. Kokoouline, E. Luc-Koenig, and F. Masnou-Seeuws, J. Phys. B **34**, L27 (2001).
[16] V. Kokoouline, O. Dulieu, R. Kosloff, and F. Masnou-Seeuws, Phys. Rev. A **62**, 032 716 (2000).
[17] D. Comparat, C. Drag, A. Fioretti, O. Dulieu, and P. Pillet, J. Mol. Spectrosc. **195**, 229 (1999).
[18] A. Fioretti, D. Comparat, C. Drag, C. Amiot, O. Dulieu, F. Masnou-Seeuws, and P. Pillet, Eur. Phys. J. D **5**, 389 (1999).
[19] C. Drag, B. Laburthe Tolra, O. Dulieu, D. Comparat, M. Vatasescu, S. Boussen, S. Guibal, A. Crubellier, and P. Pillet, IEEE J. Quantum Electron. **36**, 1378 (2000).
[20] M. Vatasescu, O. Dulieu, C. Amiot, D. Comparat, C. Drag, V. Kokoouline, F. Masnou-Seeuws, and P. Pillet, Phys. Rev. A **61**, 044 701 (2000).
[21] O. Dulieu, P. Julienne, and J. Weiner, Phys. Rev. A **49**, 607 (1994).
[22] N. Spies, Ph.D thesis, Fachbereich Chemie, Universität Kaiserslautern, 1989.
[23] M. Foucrault, Ph. Millié, and J. P. Daudey, J. Chem. Phys. **96**, 1257 (1992).
[24] C. M. Dion, C. Drag, O. Dulieu, B. Laburthe Tolra, F. Masnou-Seeuws, and P. Pillet, Phys. Rev. Lett. **86**, 2253 (2001).

[25] S. Gerstenkorn, J. Vergès, and J. Chevillard, *Atlas du Spectre d'Absorbtion de la Molecule d'Iode* (Laboratoire Aimé Cotton, Orsay, France, 1982).
[26] M. Movre and G. Pichler, J. Phys. B **10**, 2631 (1977).
[27] P. S. Julienne and J. Vigué, Phys. Rev. A **44**, 4464 (1991).
[28] M. Marinescu and A. Dalgarno, Z. Phys. D: At., Mol. Clusters **36**, 239 (1996).
[29] L. Young, W. T. Hill III, S. J. Sibener, S. D. Price, C. E. Tanner, C. E. Wieman, and S. R. Leone, Phys. Rev. A **50**, 2174 (1994).
[30] A. Giusti-Suzor and U. Fano, J. Phys. B **17**, 215 (1984).
[31] H. Friedrich, *Theoretical Atomic Physics* (Springer, New York, 1998).
[32] J. P. Burke, C. H. Greene, and J. L. Bohn, Phys. Rev. Lett. **81**, 3355 (1998).
[33] F. H. Mies and M. Raoult, Phys. Rev. A **62**, 012 708 (2000).
[34] C. Boisseau, E. Audouard, and J. Vigue, Europhys. Lett. **41**, 349 (1998).
[35] J. Trost, C. Eltschka, and H. Friedrich, Europhys. Lett. **43**, 230 (1998).
[36] U. Fano and A. R. P. Rau, *Atomic Collisions and Spectra* (Academic Press, New York, 1986).
[37] E. I. Dashevskaja and E. E. Nikitin, Can. J. Phys. **54**, 709 (1976).
[38] A. Fioretti, J. H. Muller, P. Verkerk, M. Allegrini, E. Arimondo, and P. S. Julienne, Phys. Rev. A **55**, R3999 (1997).
[39] A. Fioretti, E. Arimondo, and A. Crubellier, Eur. Phys. J. D **12**, 219 (2000).